Electronic Supplementary Material (ESI) for CrystEngComm.

Supplementary Information

Tuning the Mechanical Properties of Dicyanamide-Based Molecular Perovskites

Shivani Grover,[‡a] Stefan Burger,[‡b] Keith T. Butler,[c] Karina Hemmer,[b] Pia Vervoorts,[b] Gregor Kieslich*[b] and Ricardo Grau-Crespo*[a]

[a] *Department of Chemistry, Food and Pharmacy, University of Reading, United Kingdom, RG66DX, UK.*

[b] *Department of Chemistry, Technical University of Munich, Lichtenbergstraße 4, 85748 Garching, GER.*

[c] *Materials Research Institute, School of Engineering and Materials Science, Queen Mary University of London, Mile End Road, London E1 4NS, UK.*

[‡] Shared contribution

AUTHOR INFORMATION

Corresponding Authors

*r.grau-crespo@reading.ac.uk

*gregor.kieslich@tum.de

Theoretical calculations

Bulk Modulus - Birch-Murnaghan equation of state.
We use a third-order Birch-Murnaghan equation of state [1, 2] with energy *E* as function of volume *V*:

$$E(V) = E_0 + \frac{9V_0B}{16}\left\{\left[\left(\frac{V_0}{V}\right)^{\frac{2}{3}} - 1\right]^3 B' + \left[\left(\frac{V_0}{V}\right)^{\frac{2}{3}} - 1\right]^2 \left[6 - 4\left(\frac{V_0}{V}\right)^{\frac{2}{3}}\right]\right\}$$

where V_0 is the equilibrium volume, B is the bulk modulus, B' is the derivative of the bulk modulus with respect to pressure, and E_0 is the energy at the equilibrium volume. The bulk moduli is computed by fitting the DFT energy (E) vs. volume (V) points to the above equation. For each point the structure was relaxed by optimising cell parameters and ionic coordinates at a fixed volume. We found that the fitting was largely insensitive to the value of pressure derivative, so we fixed it at B'= 4.0 for all compositions, which is equivalent to using a second-order equation of state. The fitted energy vs. volume curves are shown in Figure S-1. The employed equation of state describes the energy variation adequately.

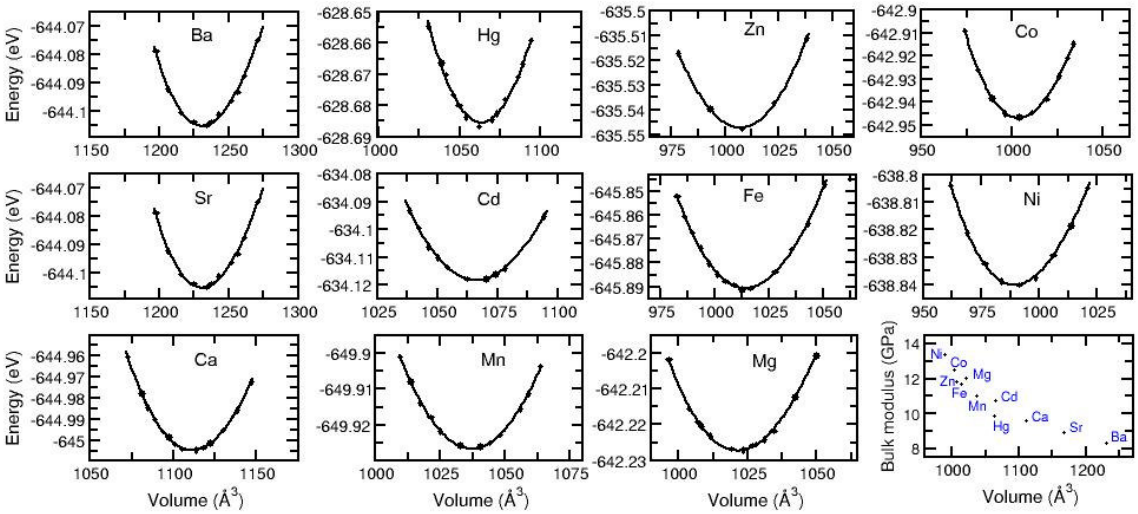

Figure S-1. Fitted energy-volume curves from DFT calculations for $[N(C_3H_7)_3CH_3]M(C_2N_3)_3$ perovskites. The final frame represents the bulk moduli vs. the equilibrium volume in each case.

Table S-1 shows the equilibrium cell parameters at zero pressure and temperature, together with the bulk moduli (B) and the linear (K) and volumetric (K_V) compressibilities obtained from the DFT simulations:

$$K = -\frac{1}{a_0}\frac{\partial a}{\partial p}$$

$$K_V = -\frac{1}{V_0}\frac{\partial V}{\partial p}$$

Tab. S-1. Equilibrium cell parameters (a_0, α_0) and volume (V_0) at zero pressure and temperature. as calculated from DFT; and the corresponding bulk moduli (B) and linear and volumetric (K_V) compressibilities.

Metal M	a_0 / Å	α_0 / degrees	V_0 / Å^3	B / GPa	K / TPa^{-1}	K_V (TPa^{-1})
Ni	10.21	76.76	989.5	13.4	25.3	75.9
Co	10.24	77.13	1003.5	12.5	26.7	80.0
Zn	10.26	76.91	1007.3	11.8	28.0	84.1
Fe	10.27	77.24	1014.2	11.7	28.5	85.6
Mg	10.31	77.00	1021.5	12.0	27.7	83.1
Mn	10.35	77.25	1037.3	11.0	30.2	90.5
Cd	10.44	77.49	1065.8	10.7	30.8	92.4
Hg	10.44	77.16	1063.6	9.9	33.8	101.2
Ca	10.56	78.23	1111.5	9.5	34.3	102.7
Sr	10.71	78.98	1167.6	8.9	36.7	109.9
Ba	10.87	79.75	1230.8	8.3	40.7	122.1

Experimental Procedures

General information.
The molecular perovskite materials were synthesised according to a strategy established in our labs, as described in the literature[3].

Powder diffraction data using Synchrotron radiation.
High-pressure powder X-ray (HPPXRD) data were collected at the Diamond Light Source (beamline I15) within beamtime CY22477-2 using an X-ray energy of 29.2 keV (λ = 0.4246 Å) and a 2D PerkinElmer area detector for data collection. A high pressure cell was used to apply hydrostatic pressure to the sample during data collection, which is described in detail at https://www.imperial.ac.uk/pressurecell/ and refs [4-6]. The pestled samples were loaded into a PTFE plastic capillary (inside diameter 1.8 mm) together with Silicone oil AP 100 as pressure transmitting medium (which is known to keep hydrostatic conditions up to pressure of 0.9 GPa) and sealed with Araldyte-2014-1 clue. In total, 17 HPPXRD pattern were collected between p = ambient and p = 0.40 GPa including one after releasing the pressure to prove reversibility. For all samples reversibility of compression was confirmed. The step size was chosen to be Δp = 0.025 GPa.
All obtained Powder X-Ray diffraction patterns were analysed by performing a Pawley profile fit analysis using TOPAS Academic v6 in combination with jEdit for creating the input files [7, 8]. Standard deviations of all parameters were calculated, and by using "randomise_on_errors", it was ensured that the minimum of the refinement was reached.

Bulk Modulus - Birch-Murnaghan equation of state
For extraction of the bulk moduli K of the materials, the obtained cell volume data from the powder diffraction experiments were plotted against the applied pressure and fitted with a 2nd-order Birch-Murnaghan equation of state (BM EoS). Standard deviations of the lattice parameters and volumes which were obtained during the Pawley profile analysis were included in the fitting process of the V(p) data with the software EoSFIT-7c [9]. For the applied pressure a standard deviation of σp = 0.002 GPa was included in the calculation. As indicated in the norm. pressure F to strain f plots, a phase transition for the Mn- and Co-containing material can be anticipated. Therefore, the bulk moduli were calculated with the appropriate pressure points for the high-pressure/low-temperature phase.
The functionality of the pressure cell set-up throughout the allocated beamtime was verified by determining the bulk moduli of two known reference materials, KBr and NiDMG. The calculated bulk moduli match the literature values very well and the procedure is described in detail in reference[4].

Powder X-Ray diffraction data
All three materials $[(n\mathrm{Pr})_3(CH_3)N]M(C_2N_3)_3$ (M = Mn^{2+}, Co^{2+}, Ni^{2+}) were thermally converted from the as-synthesised orthorhombic polymorph (*Pnma*) into the rhombohedral polymorph (*R*3*c*) prior to the diffraction experiment, as it is well described in the literature[3]. In case of the Cobalt- and the Nickel analogous, residual traces of the orthorhombic phase could be identified in the powder diffraction pattern, which was considered during the Pawley profile fitting process. The following tables only show cell parameters for the rhombohedral phase; however, the contour plots visualise *hkl* indices for both phases, where appropriate, to ensure that all reflections in the experimental pattern are assigned to the respective phase.

Tab. S-2. Pawley profile fit outcome of refined cell parameters and deviations for $[(n\mathrm{Pr})_3(CH_3)N]Mn(C_2N_3)_3$ at different pressures, ranging from ambient to p = 0.4 GPa. At the bottom, output data of PASCal - principal axis strain calculations [10] with direction of projections of the three principal axes on the unit cell axes *a, b* and *c* is shown. Reported are the median compressibilities *K* with respective errors *σK*.

p / GPa	r_wp	*a* / Å	*c* / Å	*V* / Å³
0.0001	1.26702	12.8110(1)	22.6791(4)	3223.45(8)
0.0250	1.39462	12.8121(2)	22.6259(4)	3216.45(10)
0.0500	1.48570	12.8052(2)	22.5755(4)	3205.83(9)
0.0750	1.23549	12.7975(1)	22.5207(3)	3194.21(8)
0.1000	1.30935	12.7842(1)	22.4444(4)	3176.76(8)
0.1250	1.29589	12.7750(1)	22.3711(4)	3161.83(9)
0.1500	1.17781	12.7674(1)	22.3050(4)	3148.75(9)
0.1750	1.24627	12.7648(1)	22.2593(6)	3141.00(11)
0.2000	1.29082	12.7509(2)	22.2032(6)	3126.26(11)
0.2250	1.45353	12.7434(2)	22.1566(8)	3116.03(13)
0.2500	1.23468	12.7358(2)	22.1176(10)	3106.84(16)
0.2750	1.41414	12.7281(2)	22.0942(16)	3099.82(24)
0.3000	1.39222	12.7196(2)	22.0459(17)	3088.92(26)
0.3250	1.33689	12.7130(2)	22.0008(15)	3079.38(22)
0.3500	1.29175	12.7050(2)	21.9697(14)	3071.19(21)
0.3750	1.32574	12.6988(2)	21.9389(10)	3063.88(17)
0.4000	1.45667	12.6900(2)	21.9162(14)	3056.45(21)

Axes	K/ (TPa)$^{-1}$	σK / (TPa)$^{-1}$	*a*	*b*	*c*
X_1	80.3727	2.8871	0.0000	0.0000	1.0000
X_2	25.6881	0.7233	-0.7071	-0.7071	0.0000
X_3	25.6881	0.7233	0.7071	-0.7071	0.0000
V	136.1786	3.4448			

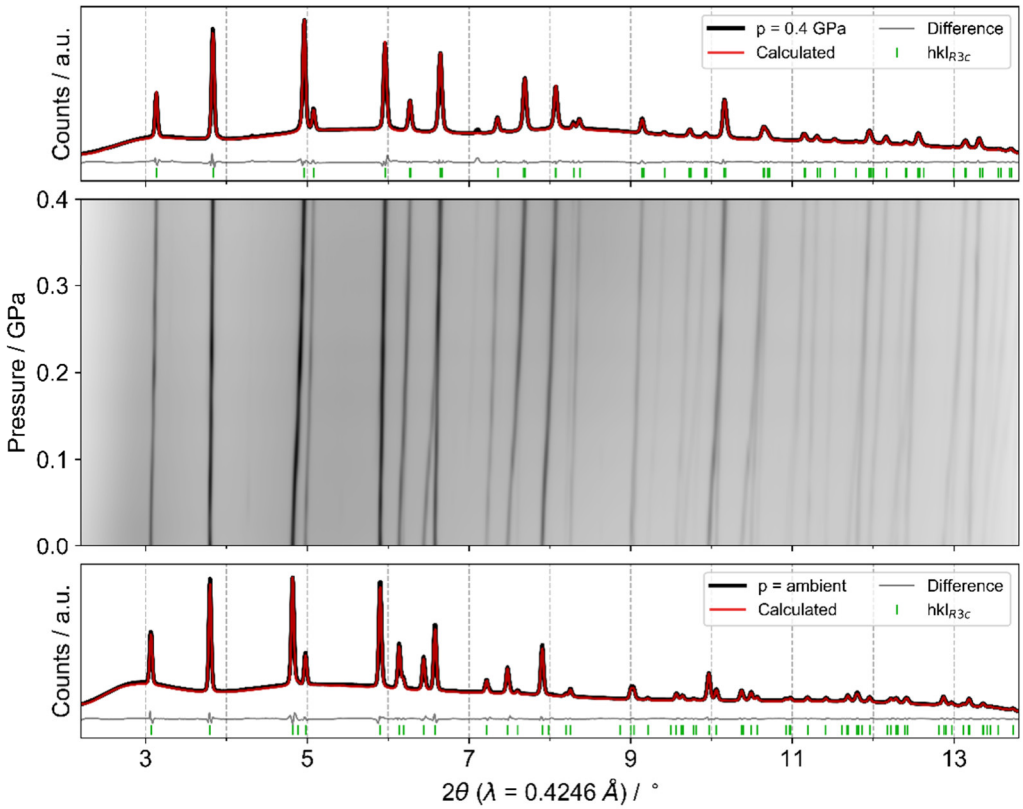

Figure S-2. HPPXRD analysis of $[(n\mathrm{Pr})_3(CH_3)N]Mn(C_2N_3)_3$ from ambient pressures to 0.4 GPa. The middle shows a contour plot of the pressure dependent diffraction patterns with intense colour corresponding to a strong reflection. Additionally, a Pawley profile fit of the patterns at ambient conditions as well as at the final pressure is shown to prove for phase purity.

Tab. S-3. Pawley profile fit outcome of refined cell parameters and deviations for $[(n\mathrm{Pr})_3(CH_3)N]Co(C_2N_3)_3$ at different pressures, ranging from ambient to p = 0.4 GPa. At the bottom, output data of PASCal - principal axis strain calculations[10] with direction of projections of the three principal axes on the unit cell axes *a, b* and *c* is shown. Reported are the median compressibilities *K* with respective errors *σK*.

p / GPa	r_wp	*a* / Å	*c* / Å	*V* / Å³
0.0001	1.24116	12.6783(3)	22.2548(7)	3097.94(16)
0.0250	0.86059	12.6752(2)	22.1793(7)	3085.95(15)
0.0500	0.73018	12.6724(3)	22.1311(6)	3077.88(14)
0.0750	0.67945	12.6650(2)	22.0888(6)	3068.43(13)
0.1000	0.83940	12.6667(3)	22.0575(8)	3064.85(17)
0.1250	0.68913	12.6598(2)	22.0303(8)	3057.76(14)
0.1500	0.64338	12.6496(2)	21.9890(11)	3047.12(18)
0.1750	0.66756	12.6449(2)	21.9491(13)	3039.35(21)
0.2000	0.77087	12.6358(3)	21.9179(14)	3030.63(24)
0.2250	0.70785	12.6309(2)	21.8913(14)	3024.60(22)
0.2500	0.75586	12.6279(3)	21.8517(14)	3017.73(22)
0.2750	0.66911	12.6227(2)	21.8309(10)	3012.34(17)
0.3000	0.69694	12.6169(2)	21.8033(12)	3005.80(19)
0.3250	0.74042	12.6099(2)	21.7811(12)	2999.37(20)
0.3500	0.76696	12.6021(2)	21.7475(8)	2991.05(15)
0.3750	0.75124	12.5958(2)	21.7268(8)	2985.24(14)
0.4000	0.83585	12.5993(2)	21.7229(8)	2986.33(14)

Axes	*K*/ (TPa)$^{-1}$	*σK* / (TPa)$^{-1}$	*a*	*b*	*c*
X_1	52.9545	0.9249	0.0000	0.0000	1.0000
X_2	17.5806	0.6632	-0.0005	1.0000	0.0000
X_3	17.5806	0.6633	0.8943	0.4475	0.0000
V	93.2264	2.5061			

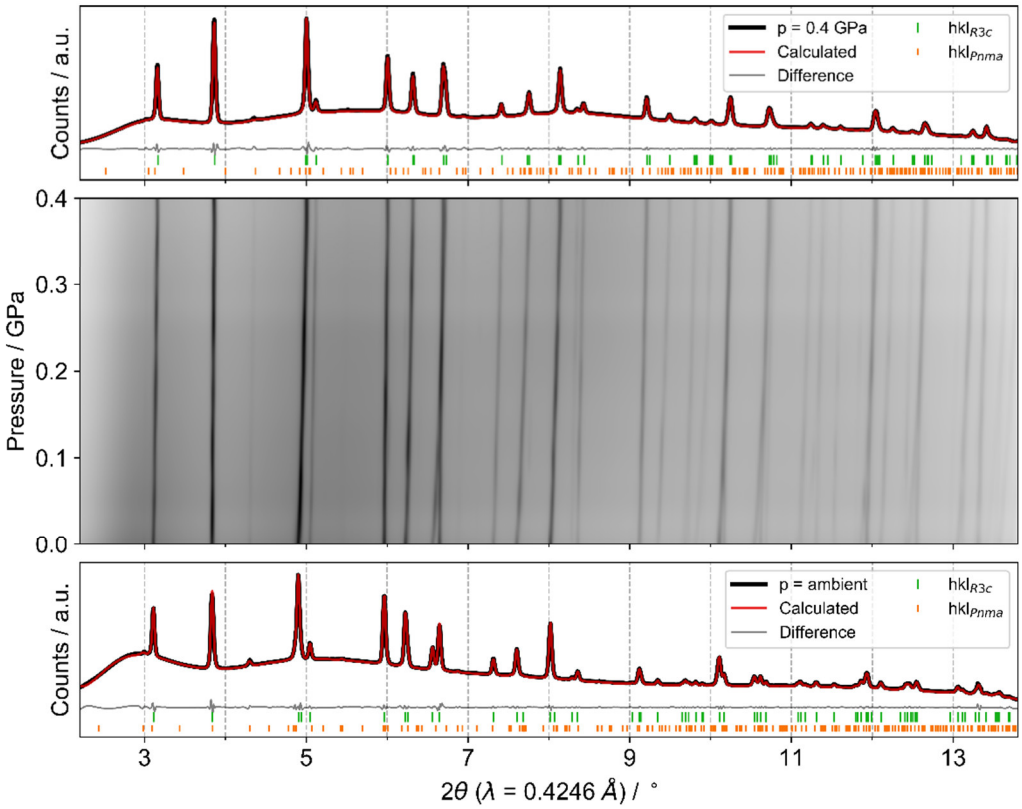

Figure S-3. HPPXRD analysis of $[(n\mathrm{Pr})_3(CH_3)N]Co(C_2N_3)_3$ from ambient pressures to 0.4 GPa. The middle shows a contour plot of the pressure dependent diffraction patterns with intense colour corresponding to a strong reflection. Additionally, a Pawley profile fit of the patterns at ambient conditions as well as at the final pressure is shown to prove for phase purity.

Tab. S-4. Pawley profile fit outcome of refined cell parameters and deviations for $[(n\mathrm{Pr})_3(CH_3)N]Ni(C_2N_3)_3$ at different pressures, ranging from ambient to p = 0.4 GPa. At the bottom, output data of PASCal - principal axis strain calculations[10] with direction of projections of the three principal axes on the unit cell axes *a, b* and *c* is shown. Reported are the median compressibilities *K* with respective errors *σK*.

p / GPa	r_wp	*a* / Å	*c* / Å	*V* / Å³
0.0001	1.55532	12.6035(2)	22.1114(6)	3041.77(12)
0.0250	1.47999	12.5989(2)	22.0755(6)	3034.63(13)
0.0500	1.57006	12.5908(2)	22.0420(7)	3026.13(13)
0.0750	1.37025	12.5846(2)	22.0066(6)	3018.30(12)
0.1000	1.23712	12.5838(1)	21.9709(5)	3013.00(09)
0.1250	1.27594	12.5789(2)	21.9435(7)	3006.91(12)
0.1500	1.17245	12.5749(2)	21.9084(7)	3000.21(13)
0.1750	1.19148	12.5676(2)	21.8795(5)	2992.74(11)
0.2000	1.30097	12.5566(2)	21.8424(6)	2982.45(13)
0.2250	1.57405	12.5570(3)	21.8221(10)	2979.88(19)
0.2500	1.17840	12.5498(3)	21.8072(9)	2974.44(17)
0.2750	1.78251	12.5503(2)	21.7838(11)	2971.46(19)
0.3000	1.81037	12.5464(3)	21.7721(14)	2968.04(25)
0.3250	1.43181	12.5320(3)	21.7307(13)	2955.58(21)
0.3500	1.32149	12.5262(3)	21.7057(10)	2949.45(18)
0.3750	1.62886	12.5202(7)	21.7079(15)	2946.96(38)
0.4000	1.78734	12.5106(8)	21.6882(18)	2939.76(45)

Axes	*K*/ $(TPa)^{-1}$	*σK* / $(TPa)^{-1}$	*a*	*b*	*c*
X_1	43.7922	1.1561	0.0000	0.0000	1.0000
X_2	17.7272	1.3559	-0.9907	-0.1362	0.0000
X_3	17.7250	1.3592	0.3628	0.9319	0.0000
V	82.8543	1.4220			

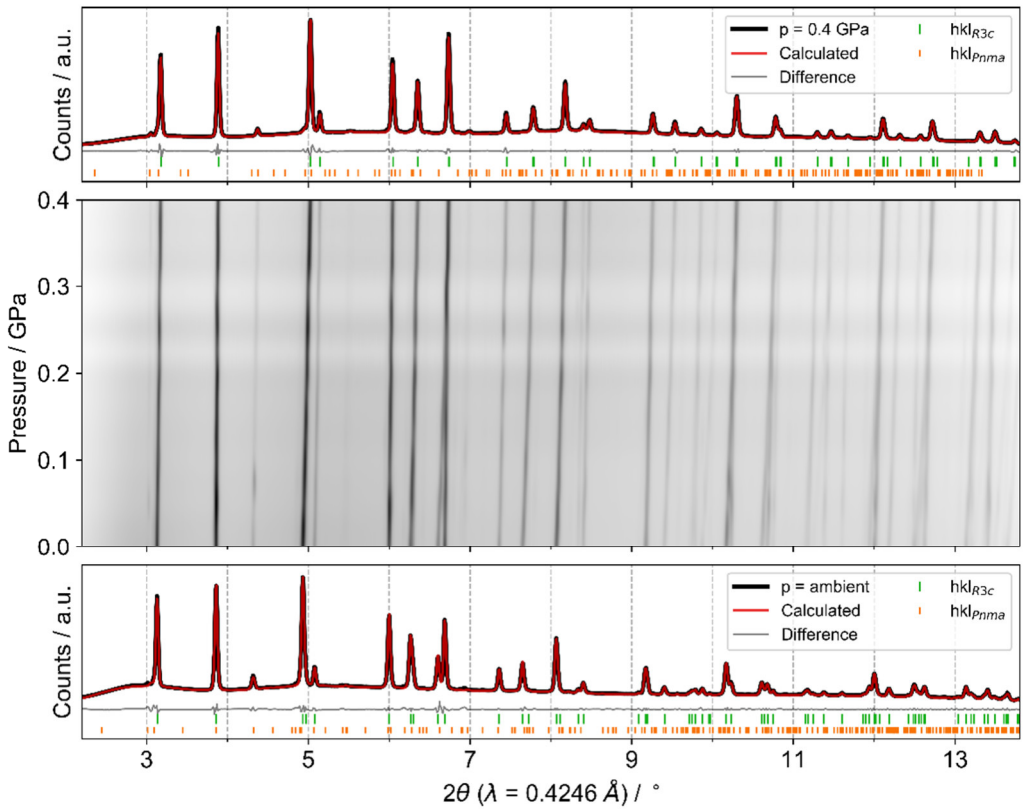

Figure S-4. HPPXRD analysis of $[(n\mathrm{Pr})_3(CH_3)N]Ni(C_2N_3)_3$ from ambient pressures to 0.4 GPa. The middle shows a contour plot of the pressure dependent diffraction patterns with intense colour corresponding to a strong reflection. Additionally, a Pawley profile fit of the patterns at ambient conditions as well as at the final pressure is shown to prove for phase purity.

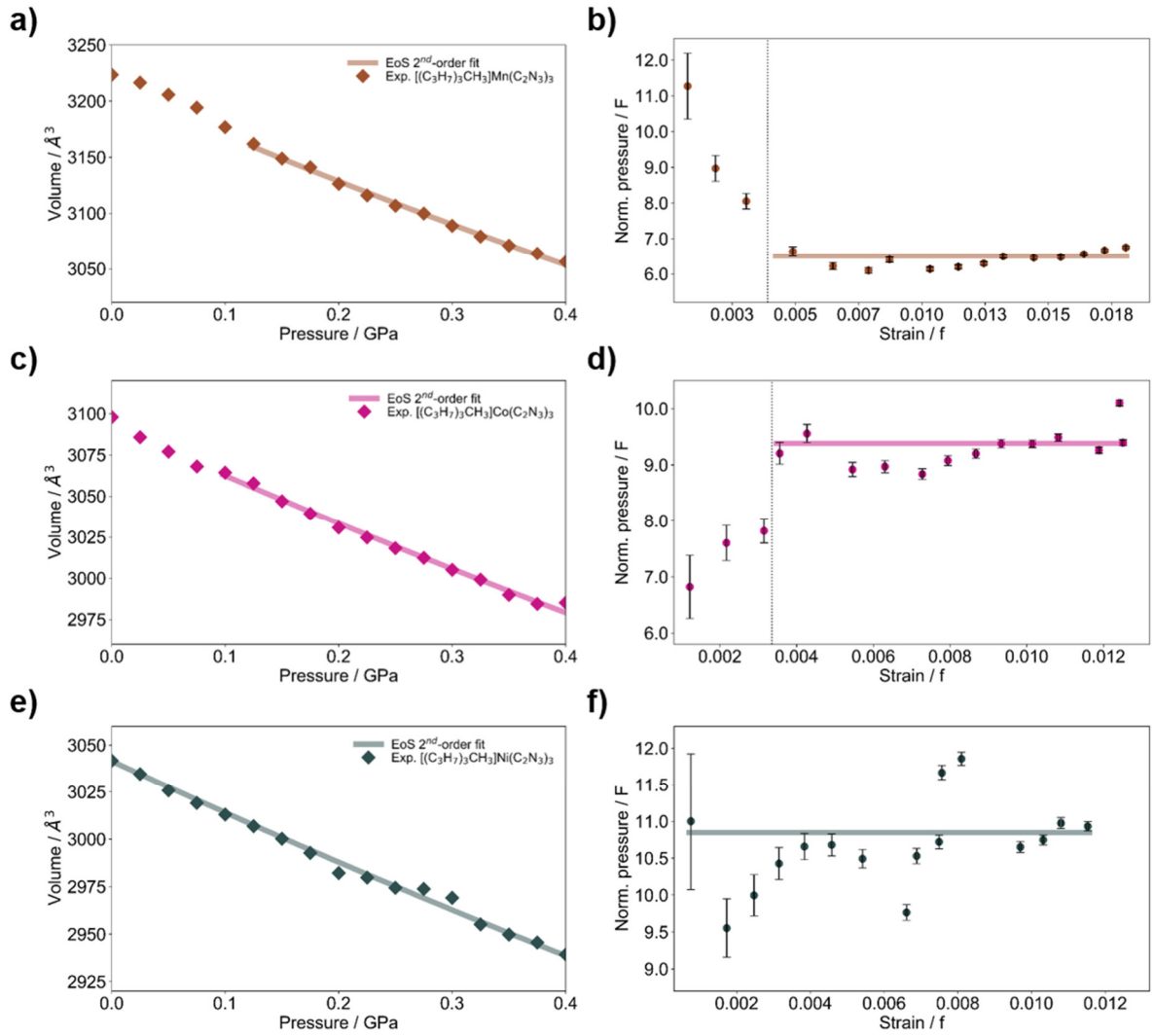

Figure S-5. Panels a) to f) show the Birch-Murnaghan equation of state of second order for the three materials, respectively, fitted to p-V data from the HPPXRD experiments with the norm. pressure to strain plots to ensure feasibility of the bulk modulus analysis. For M = Mn^{2+} and Co^{2+} the high-pressure phase transition is proposed to resemble the temperature induced phase transition which agrees with the analysis of HPPXRD pattern. The phase transitions are most visible in the Ff-plots and are indicated with a dotted line for b) and d), for which the analysis was carried out only for the high-pressure data points. Colour code: Mn – brown, Co – pink, Ni – grey.

Tab. S-5. Overview of calculated bulk moduli *B*, *B'* and refined V_0 including the estimated standard deviation obtained from pressure-dependent diffraction data of $[(n\mathrm{Pr})_3(CH_3)N]M(C_2N_3)_3$ with *M* being Manganese, Cobalt and Nickel. For M = Mn^{2+} and Co^{2+}, the bulk moduli were extracted from the high-pressure phase as indicated in b) and d) in Figure S-5. The phase transition occurs at *p* = 0.125 GPa (Mn^{2+}) and 0.1 GPa (Co^{2+}). For M = Ni^{2+} no indication of a phase transition is evident in the Ff-Plot, despite a clear peak movement in the contour plots, and therefore, the full HPPXRD dataset was used to derive the bulk modulus.

$[(n\mathrm{Pr})_3(CH_3)N]M(C_2N_3)_3$	*M* = Mn^{2+}	*M* = Co^{2+}	*M* = Ni^{2+}
B / GPa	7.08	9.90	10.85
σB / GPa	0.15	0.30	0.16
B'	4.00	4.00	4.00
V_0 / Å³	3213.4(22)	3092.9(23)	3041.5(6)

References

1. Murnaghan, F.D. Proceedings of the National Academy of Sciences, 1944. **30**(9): p. 244-247.
2. Birch, F. Physical Review, 1947. **71**(11): p. 809-824.
3. Burger, S., S. Grover, K.T. Butler, H.L.B. Boström, R. Grau-Crespo, and G. Kieslich. Materials Horizons, 2021. **8**(9): p. 2444-2450.
4. Vervoorts, P., J. Keupp, A. Schneemann, C.L. Hobday, D. Daisenberger, R.A. Fischer, R. Schmid, and G. Kieslich. Angewandte Chemie International Edition, 2021. **60**(2): p. 787-793.
5. Dissegna, S., P. Vervoorts, C.L. Hobday, T. Düren, D. Daisenberger, A.J. Smith, R.A. Fischer, and G. Kieslich. Journal of the American Chemical Society, 2018. **140**(37): p. 11581-11584.
6. Brooks, N.J., B.L.L.E. Gauthe, N.J. Terrill, S.E. Rogers, R.H. Templer, O. Ces, and J.M. Seddon. Review of Scientific Instruments, 2010. **81**(6): p. 064103.
7. Pawley, G.S. Journal of Applied Crystallography, 1981. **14**(6): p. 357-361.
8. Coelho, A. Journal of Applied Crystallography, 2018. **51**(1): p. 210-218.
9. Angel, R.J., M. Alvaro, and J. Gonzalez-Platas. 2014. **229**(5): p. 405-419.
10. Cliffe, M.J. and A.L. Goodwin. Journal of Applied Crystallography, 2012. **45**(6): p. 1321-1329.